Annals of Biomedical Engineering, Vol. 49, No. 1, January 2021 *(© 2020)* pp. 354–366
https://doi.org/10.1007/s10439-020-02557-2

Original Article

Automatic Detection of Contracting Muscle Regions via the Deformation Field of Transverse Ultrasound Images: A Feasibility Study

YANG ZHENG, HENRY SHIN, DEREK G. KAMPER, and XIAOGANG HU

Joint Department of Biomedical Engineering, University of North Carolina at Chapel Hill and North Carolina State University, 116 Manning Drive, 10206B Mary Ellen Jones Bldg, Chapel Hill, NC 27599-7575, USA

(Received 9 March 2020; accepted 25 June 2020; published online 6 July 2020)

Associate Editor Joel Stitzel oversaw the review of this article.

Abstract—Accurate identification of contracting muscles can help us to understand the muscle function in both physiological and pathological conditions. Conventional electromyography (EMG) have limited access to deep muscles, crosstalk, or instability in the recordings. Accordingly, a novel framework was developed to detect contracting muscle regions based on the deformation field of transverse ultrasound images. We first estimated the muscle movements in a stepwise calculation, to derive the deformation field. We then calculated the divergence of the deformation field to locate the expanding or shrinking regions during muscle contractions. Two preliminary experiments were performed to evaluate the feasibility of the developed algorithm. Using concurrent intramuscular EMG recordings, Experiment I verified that the divergence map can capture the activity of superficial and deep muscles, when muscles were activated voluntarily or through electrical stimulation. Experiment II verified that the divergence map can only capture contracting muscles but not muscle shortening during passive movements. The results demonstrated that the divergence can individually capture the activity of muscles at different depths, and was not sensitive to muscle shortening during passive movements. The proposed framework can automatically detect the regions of contracting muscle, and could potentially serve as a tool to assess the functions of a group of muscles concurrently.

Keywords—Transverse ultrasound imaging, Muscle contraction, Muscle function, Finger muscle, Deformation estimation.

Address correspondence to Xiaogang Hu, Joint Department of Biomedical Engineering, University of North Carolina at Chapel Hill and North Carolina State University, 116 Manning Drive, 10206B Mary Ellen Jones Bldg, Chapel Hill, NC 27599-7575, USA. Electronic mail: xiaogang@unc.edu

Yang Zheng and Henry Shin have contributed equally to the study.

ABBREVIATIONS

sEMG	Surface electromyography
iEMG	Intramuscular electromyography
US	Ultrasound
DIP	Distal interphalangeal
PIP	Proximal interphalangeal
FDP	Flexor digitorum profundus
FDS	Flexor digitorum superficialis
RMS	Root mean square
fps	Frames per second
Def.	Deformation
Div.	Divergence

INTRODUCTION

The complex muscle activation patterns allow us to perform a variety of coordinated motions. On the other hand, neuromuscular disorders can affect the functionality of muscles, resulting in abnormal muscle activation patterns.[5,9] Accurate identification of the activated muscle can help us to better understand the functions of muscles in both physiological and pathological conditions. Surface electromyography (sEMG) has been widely used to measure muscle activity in both scientific and clinical settings.[12,14] However, sEMG has several limitations such as the inability to access the deep muscles[19,27] and signal cross-talk of surrounding muscles, especially for the small hand muscles.[17,26] Alternatively, intramuscular EMG (iEMG) is also used to capture muscle activity in a variety of settings.[13,25] However, several factors,

including the invasive procedure, instability of the electrode position, and a small recording volume, can limit wide applications.

Instead of detecting the electrical activity, muscle activity can also be measured by quantifying the structural and morphologic changes of the muscle during contractions. Among the different imaging modalities, ultrasound (US) imaging has been widely used to detect and measure muscle architectures *in vivo*, such as fascial length,[15] muscle thickness,[4] cross-sectional area[7] and pennation angle.[8] In addition, US imaging is recognized as an attractive technique to measure muscle activity,[2,3,10,11,29] and it can provide real-time information regarding the movement of muscle tissues under dynamic conditions.[23,24] For example, M-mode US can evaluate the activity of the lateral abdominal muscle by measuring the thickness or a change of the thickness of muscles.[2,16] B-mode US combined with a speckle tracking algorithm can measure the activity of muscles with the US transducer placed longitudinally along the fascicle direction.[3,10,29] Briefly, the algorithm estimates the tissue displacement between two consecutive US frames by cross-correlating two-dimensional (2-D) segments of the US images. Revell et al.[20] employed a 2-D variable-sized block matching algorithm to estimate the flow fields of muscle movement. Li et al.[11] utilized a primal–dual algorithm to visualize the muscle movement. All these studies characterized muscle or tendon tissue movements longitudinally. Transverse US that quantifies muscle movements in the transverse plane has also been performed, in order to capture muscle activity from a group of muscles, such as the small forearm muscles controlling wrist and finger joints.[1] Compared with muscle tissue movements longitudinally along the muscle fascicle direction, tissue movements in the transverse plane result in more complex shifting patterns of the US image which imposes a challenge to detect the activity of a particular muscle from these images. Instead, the image sequences are fed into a machine learning algorithm for prosthetic control purposes, without an explicit knowledge on the activity of individual muscles.[6] Accordingly, the purpose of the current study was to develop an automatic algorithm based on transverse US image that can capture the active regions of different finger muscles in the forearm.

When muscles contract, depending on the position of the observation plane, the muscle area in the transverse US image could either expand (close to the muscle belly) or shrink (close to the tendon), which can be tracked with a motion estimation algorithm. In this study, a novel framework was developed to estimate the muscle movements in the transverse plane and detect the activated muscles from transverse US image. Specifically, an image registration procedure was first performed using a demons algorithm,[28] which can track the displacement of muscles and generate a deformation field in the transverse plane. The resultant deformation filed has been previously applied to classify the movements of different fingers.[21] A calculation of the divergence of the deformation field allowed us to identify regions of contracting muscles based on two distinct patterns: peaks of the divergence can capture the expanding muscle regions, and the troughs can capture the shrinking muscle regions. Two preliminary experiments were performed to evaluate the feasibility of the developed algorithm. First, the flexion of individual finger joints was produced either voluntarily or through transcutaneous nerve stimulation. Concurrent transverse US imaging and iEMG recordings from finger flexors were performed. iEMG served as a reference standard of muscle activation. Second, the flexion of finger joints was produced either voluntarily or through slow passive movements (while the subject was relaxed). The deformation field and the divergence were compared between the voluntary and passive conditions. It was hypothesized that the developed algorithm can be used as an effective method to automatically identify contracting muscles at deep and superficial layers.

MATERIALS AND METHODS

Ultrasound Deformation and Divergence Calculation

For every movement event, the US image deformation between the start and end of the flexion was obtained first using a stepwise calculation. A demons image registration algorithm[28] was used to quantify the pixel-wise deformation between pairs of ultrasound images. Each US frame was a 400 × 400-pixel image in this study. Specifically, the diffeomorphic demons algorithm[30] implemented in MATLAB (*imregdemons*) was utilized to obtain a differentiable and invertible displacement vector field, which prevents physically impossible transformations from occurring, such as a folding of the image. These 2D vector fields represent the estimated "diffusion" or movement of individual pixels from one image to another. The displacement field can be considered as a mapping function ($\vec{s}$) of each pixel from the moving image (I_M) to the fixed (reference) image (I_F). That is, a mapping function applied to the moving image is approximately equal to its fixed image ($\vec{s}(I_M) \cong I_F$).Previous work used US image registration to estimate finger muscle contractions[21]; however, only the image frames from the start and end of the motion were used for the deformation calculation. In the current study, five equally spaced

images ($I_1, \ldots, I_5$) between the start and end of each flexion were extracted for each motion (Fig. 1). In general, the calculation can be generalized to other numbers of image segments. These smaller time steps were used to isolate the smaller regional deformations of the muscles through the flexion movement. The earlier image frame was considered the fixed image between each subsequent image pair, and the deformation of each step was calculated between adjacent images.

$$I_1 \underset{\vec{s}_1}{\rightarrow} I_2 \underset{\vec{s}_2}{\rightarrow} I_3 \underset{\vec{s}_3}{\rightarrow} I_4 \underset{\vec{s}_4}{\rightarrow} I_5 \tag{1}$$

With multiple sequential steps, each mapping function only represented the deformation that occurred between steps relative to the fixed image of the pair. (e.g. $\vec{s}_1$ represents the deformation of I_1 onto I_2 with respect to I_1). By applying subsequent mapping functions recursively, it was possible to transform a deformation step to the reference coordinates of a previous image.

$$\begin{aligned} \Delta_{1\rightarrow 2,I_1} &= \vec{s}_1 \\ \Delta_{2\rightarrow 3,I_1} &= \vec{s}_1(\vec{s}_2) \\ \Delta_{3\rightarrow 4,I_1} &= \vec{s}_1(\vec{s}_2(\vec{s}_3)) \\ \Delta_{4\rightarrow 5,I_1} &= \vec{s}_1(\vec{s}_2(\vec{s}_3(\vec{s}_4))) \end{aligned} \tag{2}$$

A summation of each of these smaller deformations then represented the total deformation ($\vec{F}$) that occurred between the starting and ending image frames of a single flexion motion.

$$\vec{F}_{1\rightarrow 5} = \vec{s}_1 + \vec{s}_1(\vec{s}_2) + \vec{s}_1(\vec{s}_2(\vec{s}_3)) + \vec{s}_1(\vec{s}_2(\vec{s}_3(\vec{s}_4))) \tag{3}$$

Then, the cubic root of a 400 × 400 Hann window was applied to the original image deformation ($\vec{F}_{1\rightarrow 5}$) to remove the inaccurate edge effects from the divergence calculation. The image deformation was further downsampled to a 20 × 20 deformation vector field using a bicubic interpolation function with antialiasing, in order to obtain a global estimate of the macro tissue movement. Lastly, the divergence of this downsampled deformation field was calculated to reduce the dimensionality of the deformation, i.e. from a vector field to a scalar field, which can also better quantify the regions of concentric expansion due to muscle contraction.

$$div\vec{F}_{1\rightarrow 5} = \nabla \cdot \vec{F}_{1\rightarrow 5} = \frac{\partial F_x}{\partial x} + \frac{\partial F_y}{\partial y} \tag{4}$$

The divergence of a vector field measures the flux or change of the field and is related to the magnitude of a source or sink in a fluid flow. The divergence of the deformation in our case represents the relative expansion or shrinkage of the muscle tissue at each pixel location. The 20 × 20 divergence field was then upsampled back to a 400 × 400 scalar map for a smooth appearance. Figure 1 shows an overview of all the calculation steps of the US deformation and divergence.

Experiments

The performance of the developed algorithm was evaluated preliminarily using two experiments. Experiment I was performed to verify that the divergence of the deformation field reflected the muscle activity of superficial and deep muscles. The flexion of the distal interphalangeal (DIP) joint or the proximal interphalangeal (PIP) joint were generated either voluntarily or via transcutaneous electrical nerve stimulation. To verify the activation of the corresponding muscles, iEMG recordings were acquired from the flexor digitorum profundus (FDP) muscle that flexes the DIP joints and the flexor digitorum superficialis (FDS) muscle that flexes the PIP joints, respectively. Experiment II was performed to verify that the divergence of the deformation field only captured contracting muscles but not muscle passive shortening. The same joints as in Experiment I were moved voluntarily or moved passively by an experimenter. The passive movement condition was designed to verify that our contracting muscle detection method was insensitive to passive muscle shortening (Fig. 2).

Subjects

Two neurologically intact male subjects were recruited. The two subjects participated in the two different experiments, respectively. Both subjects gave informed consent with protocols approved by the Institutional Review Board of the University of North Carolina at Chapel Hill.

Apparatus and Data Acquisition

Electrical Stimulation (Experiment I) Sixteen gel-based electrodes with a diameter of approximately 1 cm (Vermed Inc, Buffalo, NY) were arranged in a 2 × 8 array and placed near the short head of the biceps brachii on the medial side (Fig. 2a) where the median and ulnar nerve bundles are superficial. The electrode array technique has been used in our previous studies to selectively elicit flexion or extension motions of different finger joints.[22,31,32] The 16 electrodes were connected to the columns of a switch matrix (34904A; Agilent Technologies, Santa Clara, CA) and the rows of the switch matrix was connected to the anode and cathode of one channel of a programmable multi-channel stimulator (STG4008; Mul-

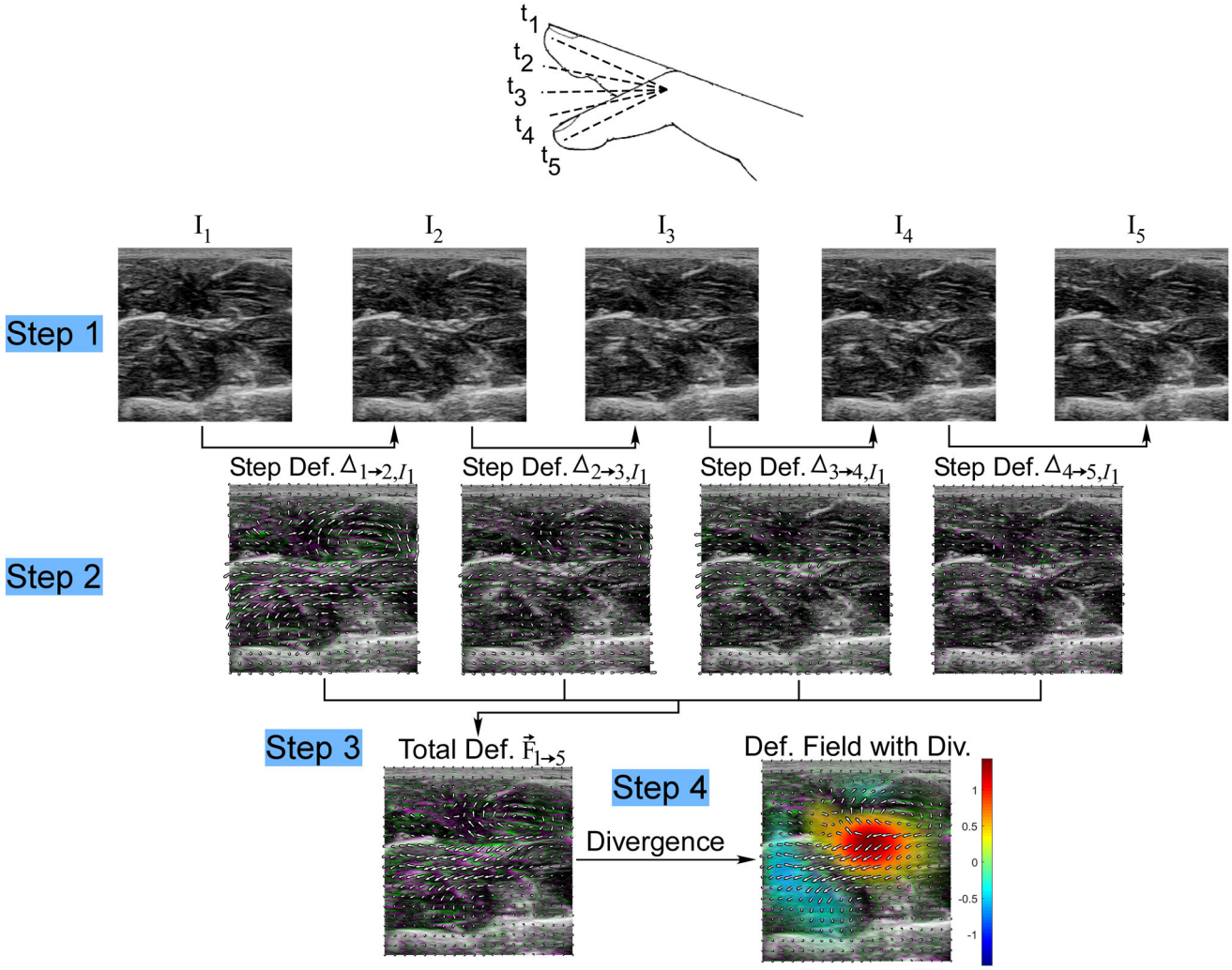

FIGURE 1. Overall procedures of ultrasound deformation and divergence calculation. Step 1, *N* (*N* = 5 in this study) equally spaced image frames ($I_1, \ldots, I_5$) between the start and end of each flexion were extracted. The size of each frame was 400 × 400 pixels in this study. Step 2, the step deformation of two adjacent images was obtained through the diffeomorphic demons algorithm and related to the reference coordinates of the first image by applying subsequent mapping functions recursively. For a clear appearance, the original 400 × 400 deformation field was downsampled to a 20 × 20 vector field using a bicubic interpolation function with antialiasing. Step 3, all the original step deformations were summed up to represent the total deformation ($\vec{F}_{1\rightarrow5}$) that occurred between the starting and ending image frames of a single flexion. The color (pale green) shown in the results of Step 2 and Step 3 represents the difference between two US images. Step 4, before calculating the divergence of the deformation field, the original deformation field was first processed using the cubic root of a 400 × 400 Hann window to remove the inaccurate edge effects from the divergence calculation and then downsampled to a 20 × 20 deformation field. The resultant divergence (color map shown in the results of Step 4) of the deformation field was upsampled back to a 400 × 400 scalar map for a smooth appearance. Numerically the divergence signifies the sources and sinks from the deformation field and is an indication of the regions of concentric expansion and shrink of tissues, respectively.

tichannel Systems, Reutlingen, Germany). The electrodes were secured in place using a custom vice that applied pressure over the electrode array into the subject's upper arm. The stimulator and the switch matrix were controlled using a custom MATLAB (version 2016b, MathWorks Inc) user-interface such that stimulation trains can be delivered to any electrode pair.

Intramuscular EMG Recordings (Experiment I) iEMG signals were detected from the FDP and FDS muscles using separate monofiler finewire electrodes (diameter: 0.05 mm; California finewire) inserted with 30-gauge hypodermic needles. The depth of the electrode was adjusted until we observed obvious muscle activity when the subject repeated the flexion of the corresponding joint but no activity when other joints moved

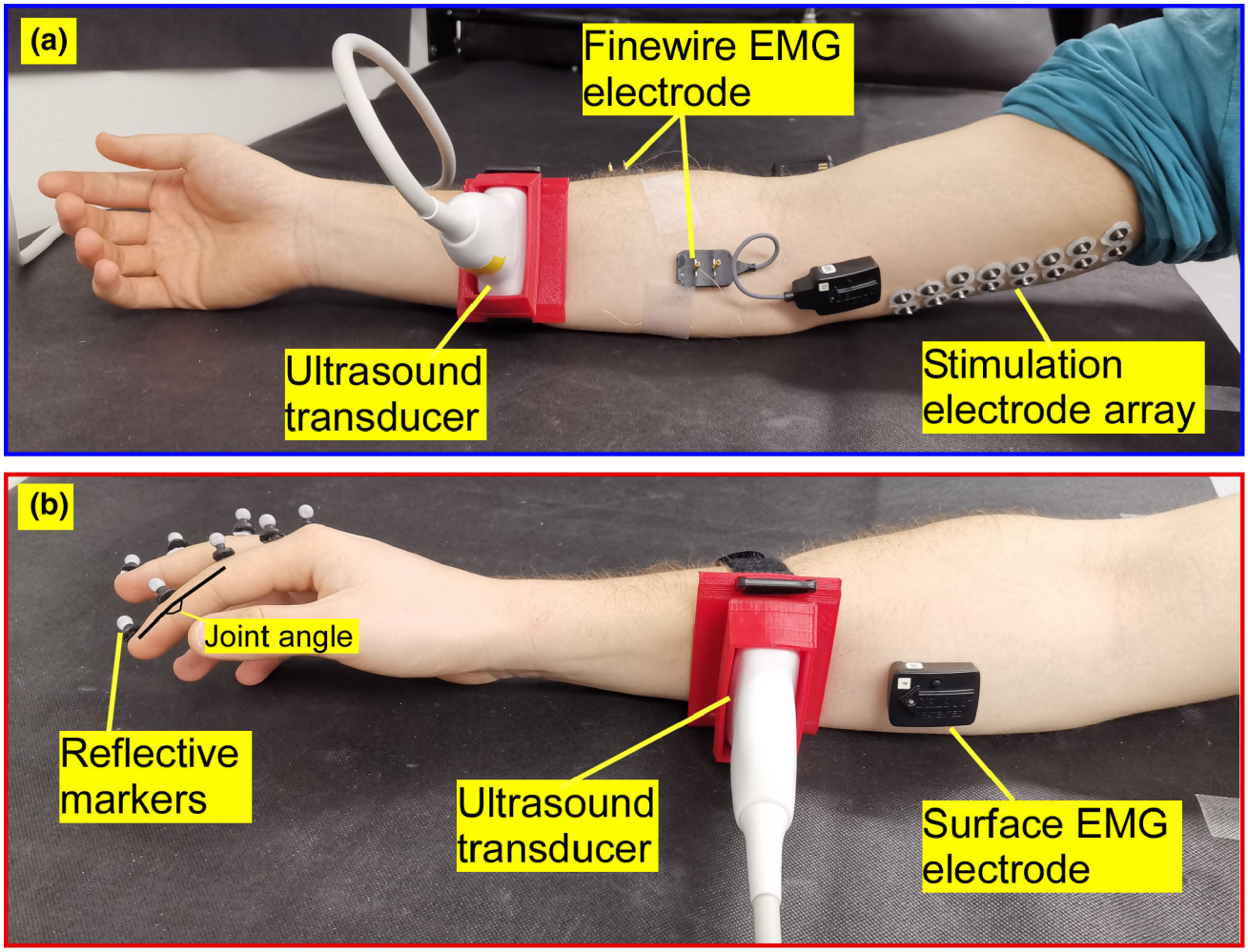

FIGURE 2. Experimental setup. Experiment I (a): transverse Ultrasound images were recorded from mid-point along the forearm. A 2 × 8 stimulation electrode array was placed beneath the short head of the biceps brachii along the ulnar/median nerve bundles to elicit various finger flexions via electrical stimulation. Two finewire EMG electrodes were inserted into the flexor digitorum profundus (FDP) and flexor digitorum superficialis (FDS) muscles respectively to capture contacting muscle activities. Experiment II (b): reflective markers were placed on the back side of hand to track the joint angle of the distal interphalangeal (DIP) and proximal interphalangeal (PIP) joints. Ultrasound images were also recorded from mid-point along the forearm. A surface EMG electrode was placed over the finger flexors to record the FDS and FDP muscle activity.

voluntarily. Monopolar signals were amplified, band-pass filtered (20–450 Hz), and sampled at 2000 Hz via the Trigno system (Delsys Inc, Natick, MA). A ground electrode was placed around the olecranon process at the elbow.

Finger Motion Tracking (Experiment II) The subject's finger kinematics were recorded using an 8-camera optical motion tracking system (Optitrack; Natural Point, Inc.). Four 6 mm IR-reflective markers were placed on the back side of the index and middle fingers to measure the angles of the DIP and PIP joints (Fig. 2b). The 3D positions of the markers were recorded in 100 frames per second (fps) (Motive; Natural Point, Inc.).

Surface EMG Recordings (Experiment II A wireless sEMG electrode (Trigno, Delsys Inc., Natick, MA) was placed over the finger flexors (Fig. 2b). The subject was requested to repeat the finger flexion. The placement of electrodes was determined initially by palpating the muscle belly of the contracting muscles, and was then fine-tuned to maximize the EMG amplitude recordings. Bipolar sEMG signals were amplified, band-pass filtered (20–450 Hz), and sampled at 2000 Hz.

Ultrasound Recordings (Experiments I and II) The transverse US images of muscle contraction were recorded using a clinical Doppler ultrasound system (S2; SonoScape Medical Corp.) with a 5–10 MHz lin-

ear array transducer (L741, SonoScape Medical Corp.). The probe was secured to the arm using a custom 3D printed holder (Figs. 2a and 2b) at midpoint (50% length) of the forearm from the cubital fossa to the wrist joint. The ultrasound images were recorded at a sampling rate of 54 fps, and then exported to MATLAB in sets of 46 × 46 mm image frames.

Synchronization of Recordings In Experiment I, the electrical stimulator, the intramuscular EMG acquisition system, and the ultrasound acquisition system were synchronized using a synchronization pulse from the stimulator. In Experiment II, the surface EMG acquisition system, the motion capture system, and the ultrasound acquisition system were synchronized using a synchronization pulse from the motion capture system.

Experimental Procedure

Both subjects were seated comfortably in a chair with their right arm resting on a table. In Experiment I, to evoke joint movements using electrical stimulation, a searching procedure was performed to select the stimulation electrode pairs and the corresponding current intensity that can elicit independent PIP or DIP joint movement of a single finger. Then, the selected electrode pair was used to elicit single PIP or DIP joint movement repeatedly in a trial, which included eight 1-s long stimulation trains with a 1-s resting time in between. Each stimulation train contained biphasic pulses with a 500-μs width at a stimulation frequency of 30 Hz. After each stimulation train, the subject was asked to voluntarily move the fingers to the same pre-stimulation baseline position. In the voluntary activation condition, the subject was requested to flex the DIP or PIP joint of a single finger repeatedly at approximately 0.5 Hz, or alternate between the DIP and PIP joints of a single finger in a trial.

In Experiment II, during passive movements, the subject was asked to be completely relaxed. An experimenter held the subject's finger and moved the finger joint slowly with a speed of approximately 25°/s. The slow movement speed was needed to avoid any reflex activities. A sensitivity analysis was performed in the Supplementary Material to determine that the rate of change of the fascicle displacement did not bias the estimation of the muscle deformation. When sEMG activities were observed, the trial was repeated. In the voluntary condition, the subject was requested to flex the PIP and DIP joints of a specific finger (at 0.5 Hz per joint) in an alternating manner in a single trial.

Data Processing

Identification of Flexion Time

Before using the US images to detect the muscle contraction regions, we first determined the timings of the start and the end of each flexion. In the electrical stimulation condition of Experiment I, the start and end times of the stimulated flexion were obtained directly from the timings of each 1-s stimulation train. In the voluntary condition of Experiment I, the start and end timings of each flexion was visually identified from the ultrasound video. In Experiment II, the timings were identified using the PIP and DIP joint kinematic data based on marker positions. The joint angle was defined in Fig. 2b. A full extension position corresponded to a joint angle of approximately 180° and joint flexion resulted in a decreased angle. The resultant joint kinematic data were then used to obtain the timings of the start and end of every voluntary/passive flexion. These flexion times were then used to extract the corresponding US image frames and iEMG/sEMG activities.

EMG Activity

EMG During Electrical Stimulation The iEMG segments that started from 0 ms and ended 33 ms after the onset of individual stimulation pulses were extracted, and the muscle compound action potentials were then averaged within each 1-s stimulation train for individual channels. Stimulation artifacts were identified manually based on the average iEMG and excluded from further analysis. The iEMG amplitude was calculated as the difference between the maximum and minimum of the average compound action potential for individual stimulation trains and individual channels.

EMG During Voluntary/Passive Joint Flexion iEMG signals from Experiment I and sEMG signals from Experiment II were first filtered with a high-pass filter (zero-phase forward and reverse digital IIR filtering) with a cut-off frequency of 50 Hz (iEMG) and 10 Hz (sEMG), respectively to remove motion artifacts. Then, the iEMG and sEMG signals were filtered with notch filters at 60 Hz and its higher order harmonics to remove the power-line noise. The amplitude (root mean square, RMS) of both iEMG and sEMG was calculated for individual flexions which were determined by the start and end of flexions.

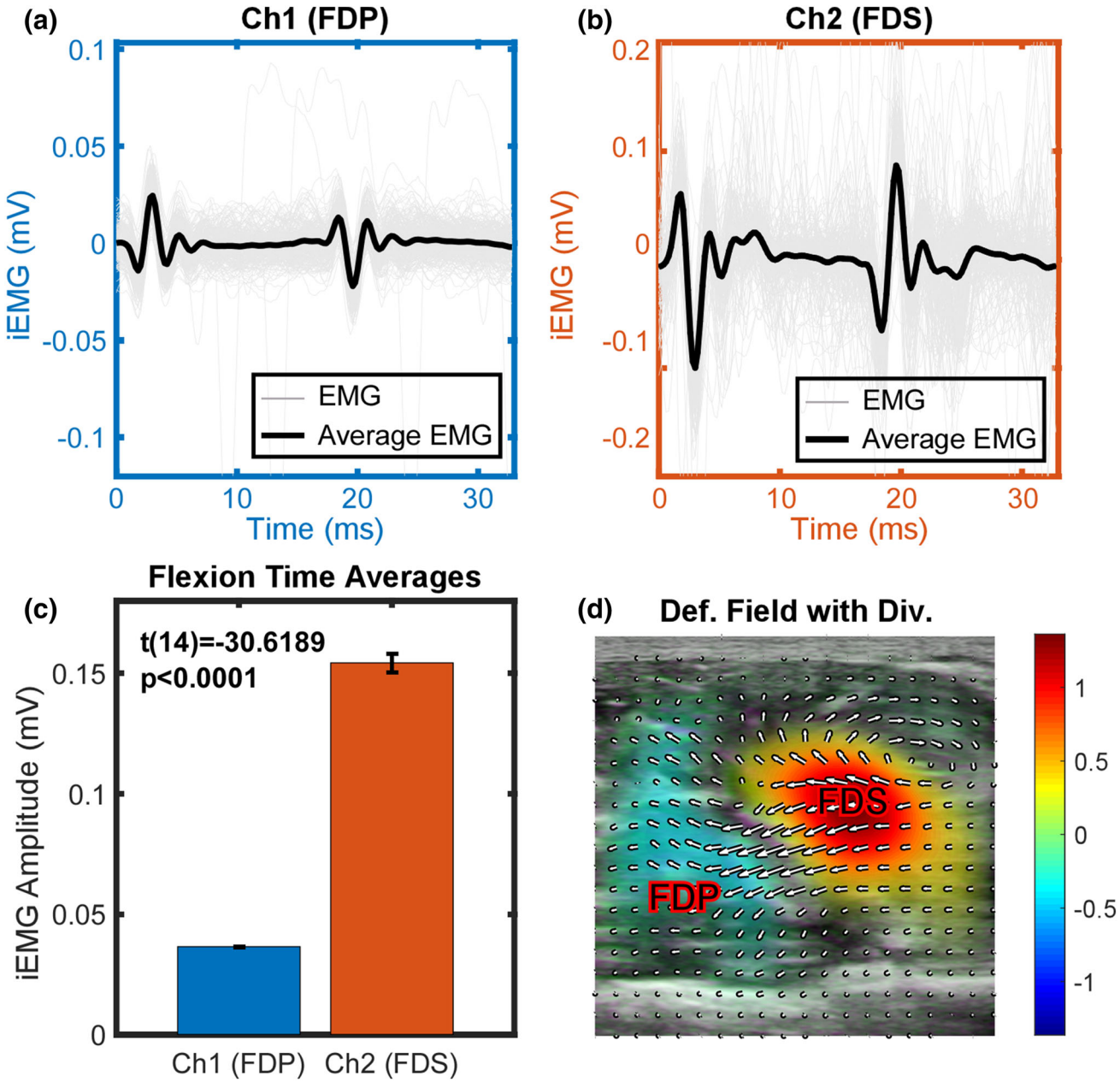

FIGURE 3. The iEMG signals and the ultrasound deformation field with divergence from an electrical stimulation trial with independent PIP flexion of the middle finger. The iEMG signals of the FDP (a) and FDS (b) muscles, respectively from eight stimulation trains of the trial. The stimulation started at 0 s. Comparison of the average iEMG amplitude between the FDS and FDP muscles (c). Error bars represent the standard error of the iEMG amplitude across individual stimulation trains. The average deformation (Def.) field of the ultrasound image and the resultant divergence (Div.) field (d).

RESULTS

Experiment I

An electrode pair was used to elicit independent PIP flexion of the middle finger. Figures 3a and 3b illustrate the iEMG signals from the trial with elicited PIP flexion of the middle finger. The stimulation started at 0 s. The thin gray lines represent the iEMG segments after the stimulation onset from all the eight stimulation trains, and the thick black lines were the average iEMG of the individual segments. The FDS muscle (channel 2) controlling the PIP flexion showed an obvious H-reflex activity at approximately 20 ms, and the FDP (channel 1) showed relatively low iEMG activity at approximately 20 ms. In order to compare the iEMG amplitude between the two channels, the average iEMG amplitude (peak-to-peak) was calculated as shown in Fig. 3c. The two-sample *t* test

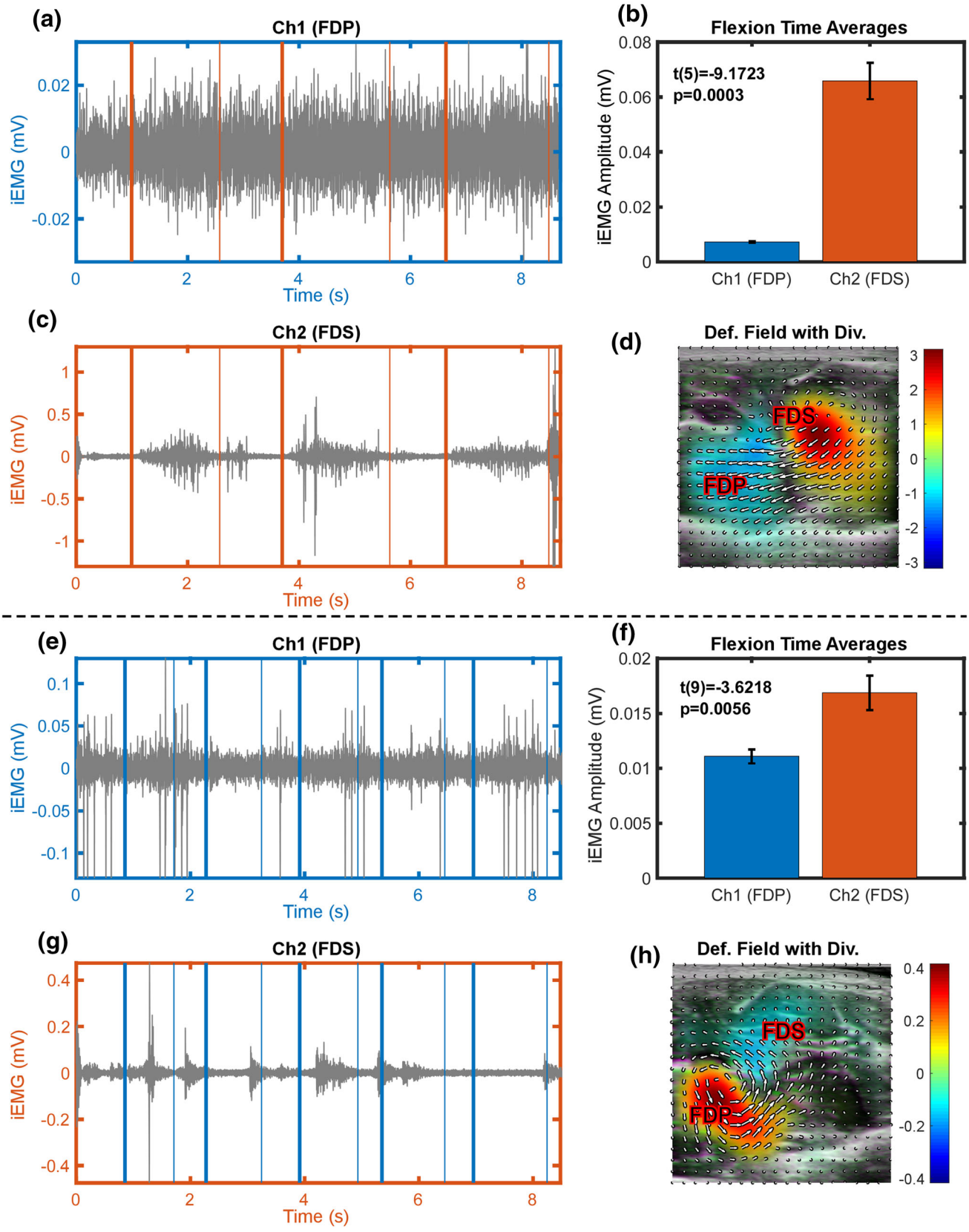
(a)
Ch1 (FDP)
iEMG (mV)
Time (s)
(b)
Flexion Time Averages
t(5)=-9.1723
p=0.0003
iEMG Amplitude (mV)
Ch1 (FDP)
Ch2 (FDS)
(c)
Ch2 (FDS)
iEMG (mV)
Time (s)
(d)
Def. Field with Div.
FDS
FDP
(e)
Ch1 (FDP)
iEMG (mV)
Time (s)
(f)
Flexion Time Averages
t(9)=-3.6218
p=0.0056
iEMG Amplitude (mV)
Ch1 (FDP)
Ch2 (FDS)
(g)
Ch2 (FDS)
iEMG (mV)
Time (s)
(h)
Def. Field with Div.
FDS
FDP

◀**FIGURE 4. The iEMG signals (a and c) and the ultrasound deformation field with divergence (d) from the trial with the voluntary independent PIP flexion. The iEMG signals (e and g) and the ultrasound deformation field with divergence (h) from the trial with the voluntary independent DIP flexion. Orange thick and thin vertical lines represent the start and end of individual PIP flexions, respectively (a, c). Blue thick and thin vertical lines represent the start and end of individual DIP flexions, respectively (e, g). The iEMG amplitude (root mean square) was calculated within individual flexions and then compared between the FDS and FDP muscles (b, f).**

showed that the iEMG amplitude of the FDS muscle was significantly higher than the FDP muscle ($t(14) = -30.6189$, $p < 0.0001$). Figure 3d illustrates the deformation field with divergence of the ultrasound image. The deformation field was obtained by averaging the deformation calculations from all flexions to reduce the sampling bias, and the divergence was calculated based on the average deformation field. The divergence with positive peak values was located at the FDS muscle area, which demonstrated that the pixels from the FDS muscle region expanded. This was consistent with the iEMG recordings that demonstrated the activation of the FDS muscle.

Figure 4 shows the results of two voluntary trials with independent PIP or DIP flexion of the middle finger, respectively. In the PIP flexion trial (Figs. 4a, 4b, 4c, and 4d), the FDS muscle showed strong muscle activities during joint flexions. Figure 4b illustrates the average iEMG amplitude (RMS) across all flexions from the two channels. The statistical analysis (paired t-test) results showed that the iEMG amplitude of the FDS was significantly larger compared with that of the FDP (0.0658 mV vs. 0.0072 mV, $t(5) = -9.1723$, $p = 0.0003$). The divergence map showed that the expansion area was located at the FDS muscle, which demonstrated the shortening and contraction of the FDS muscle (Fig. 4d), leading to a PIP flexion. In the DIP flexion trial (Figs. 4e, 4f, 4g, and 4h), the average iEMG amplitude across all flexions for the two channels is illustrated in Fig. 4f. Compared with the PIP flexion trial, the iEMG amplitude of the FDP muscle increased (from 0.0072 to 0.0111 mV) and the iEMG amplitude of the FDS muscle decreased (from 0.0658 to 0.0169 mV), even though the iEMG amplitude of the FDS muscle was still significantly higher than that of the FDP muscle ($t(9) = -3.6218$, $p = 0.0056$). The peak of the divergence map was at the FDP muscle region. This demonstrated the expansion and contraction of the FDP muscle (Fig. 4h), leading to a DIP flexion in this trial.

Figure 5 illustrates the iEMG signals and the ultrasound deformation field with divergence from the trial in which the PIP and DIP joints flexed alternately. The iEMG amplitude was calculated for individual flexions and individual channels. Figure 5b shows the average iEMG amplitude of the FDP muscle when the PIP and DIP joint flexed, respectively. The statistical analysis (paired t-test) results showed that the iEMG amplitude of the FDP muscle during the DIP flexion was significantly larger than that during the PIP flexion ($t(5) = -6.9740$, $p = 0.0009$). Figure 5e shows the average iEMG amplitude of the FDS muscle when the PIP and DIP joint flexed, respectively. The statistical analysis (paired t-test) results showed that the iEMG amplitude of the FDS muscle during the PIP flexion was significantly larger than that during the DIP flexion ($t(5) = 4.4687$, $p = 0.0066$). Consistent with the results shown in Figs. 4d and 4h, the peak of the divergence map during the PIP joint flexion and the DIP joint flexion was located at the FDS (Fig. 5c) and FDP (Fig. 5f) muscles, respectively.

Experiment II

The US deformation field with divergence between the voluntary and passive joint movement conditions was compared. Figures 6a and 6b illustrate the joint kinematics and the sEMG signal, respectively from a representative trial, with voluntary PIP and DIP joint flexions alternately. Due to the enslavement of the DIP joint movement with the PIP joint for the subject, the flexion of the DIP joint was always accompanied with the flexion of the PIP joint when the subject tried to flex the DIP joint independently (Fig. 6a). In order to simplify the description, the 'DIP flexion' condition was still used to represent the condition when the DIP joint was supposed to flex independently, even though the PIP joint also flexed simultaneously. Figures 6c and 6d illustrate the joint kinematics and the sEMG signal, respectively from a representative trial, with passive PIP and DIP joint flexions alternately. In the DIP flexion condition, both the DIP and PIP joints were passively moved to mimic the situation in the voluntary DIP flexion condition. The range of motion (the absolute difference of the joint angle between the start and end of individual flexions) was first calculated for individual joints and individual flexions, respectively, and was then summed up across the two joints. Since the range of motion during voluntary PIP flexion was significantly larger than that during passive PIP flexion, the end timing of individual voluntary PIP flexions was corrected to match the joint range of motion between the voluntary and passive conditions. The corrected timings were subsequently used for the sEMG and US image processing. The statistical analysis (two-sample t-test) results showed that the joint kinematics after correction were matched during the DIP flexion ($t(10) = -0.3697$, $p = 0.7193$) and PIP flexion ($t(11) = -0.2265$, $p = 0.8250$).

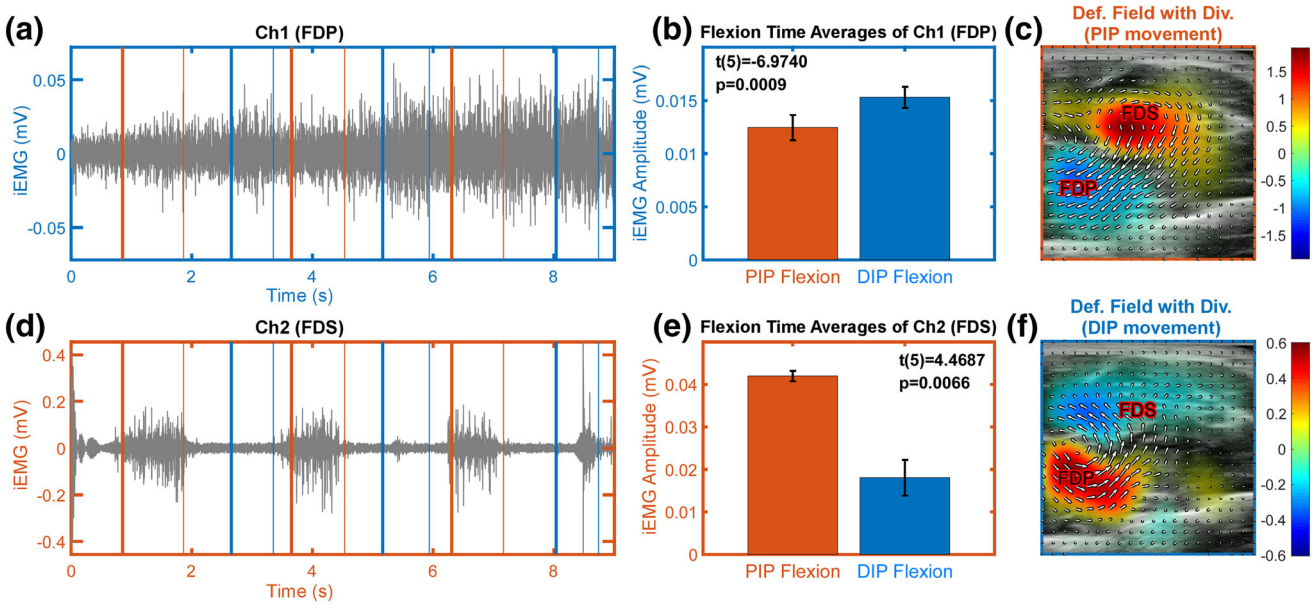

FIGURE 5. The iEMG signals and the ultrasound deformation field with divergence from the trial with the voluntary movement of the PIP and DIP joint alternately. Orange thick and thin vertical lines represent the start and end of individual PIP flexions, respectively, and blue thick and thin vertical lines represent the start and end of individual DIP flexions, respectively (a, d). The iEMG amplitude of the first channel (FDP muscle) was calculated within individual flexions and then compared between the PIP and DIP joint flexions (b). The iEMG amplitude of the second channel (FDS muscle) was calculated within individual flexions and then compared between the PIP and DIP joint flexions (e). The ultrasound deformation field with divergence when the PIP joint flexed (c). The ultrasound deformation field with divergence when the DIP joint flexed (f).

Figure 6e compares the sEMG amplitude between three different conditions, i.e. the voluntary condition, the passive condition, and the baseline condition. The sEMG amplitude of the baseline condition was calculated using the recording segment when there was no passive or voluntary joint motion. The results (two-sample t-test with Bonferroni correction) showed that the sEMG amplitude in the voluntary condition was significantly larger than the passive condition ($t(10) = -4.5460$, $p < 0.01$) and the baseline condition ($t(11) = -5.0852$, $p < 0.01$) during the DIP flexion, and there was no significant difference between the baseline condition and the passive condition ($t(7) = 0.4623$, $p > 0.05$). Similar results were obtained during the PIP flexion such that the sEMG amplitude in the voluntary condition was significantly larger than the passive condition ($t(11) = -18.9990$, $p < 0.0001$) and the baseline condition ($t(10) = -17.3265$, $p < 0.0001$), and there was no significant difference between the baseline condition and the passive condition ($t(9) = -1.0058$, $p > 0.05$).

The US deformation field with the divergence from the voluntary and passive DIP flexions is illustrated in Figs. 6f and 6h, respectively. The positive peaks of the divergence map were located at both the FDS and FDP muscles (Fig. 6f) due to the fact that both the DIP and PIP joints flexed during the DIP flexion condition. Certain regions showed a negative divergence with large absolute values, which demonstrated the shrinkage of these regions. The shrunk pixels in these regions could be caused by the expanding pixels in the surrounding regions like the FDS and FDP muscles. In the passive flexion condition (Fig. 6h), the ultrasound deformation (arrow length) was smaller compared with the deformation in the voluntary condition (Fig. 6f). As a result, the divergence map showed minimal expanding or shrinking regions, compared with the voluntary condition. Figure 6g illustrates the deformation field with divergence during voluntary PIP flexions. The contracting region of the FDS muscle shifted leftwards compared with the voluntary DIP flexion condition. Same as the passive DIP flexion condition, the deformation field and the divergence were both negligible in the passive PIP flexion condition (Fig. 6i).

DISCUSSION

This study developed a novel framework to automatically identify the contracting muscles at different depths by measuring muscle tissue movements from transverse US images without the need of invasive methods such as intramuscular EMG recordings. We first estimated the muscle tissue movements (deformation field), which was performed in a stepwise manner in order to cope with the large muscle deformation in the transverse plane. We then calculated the

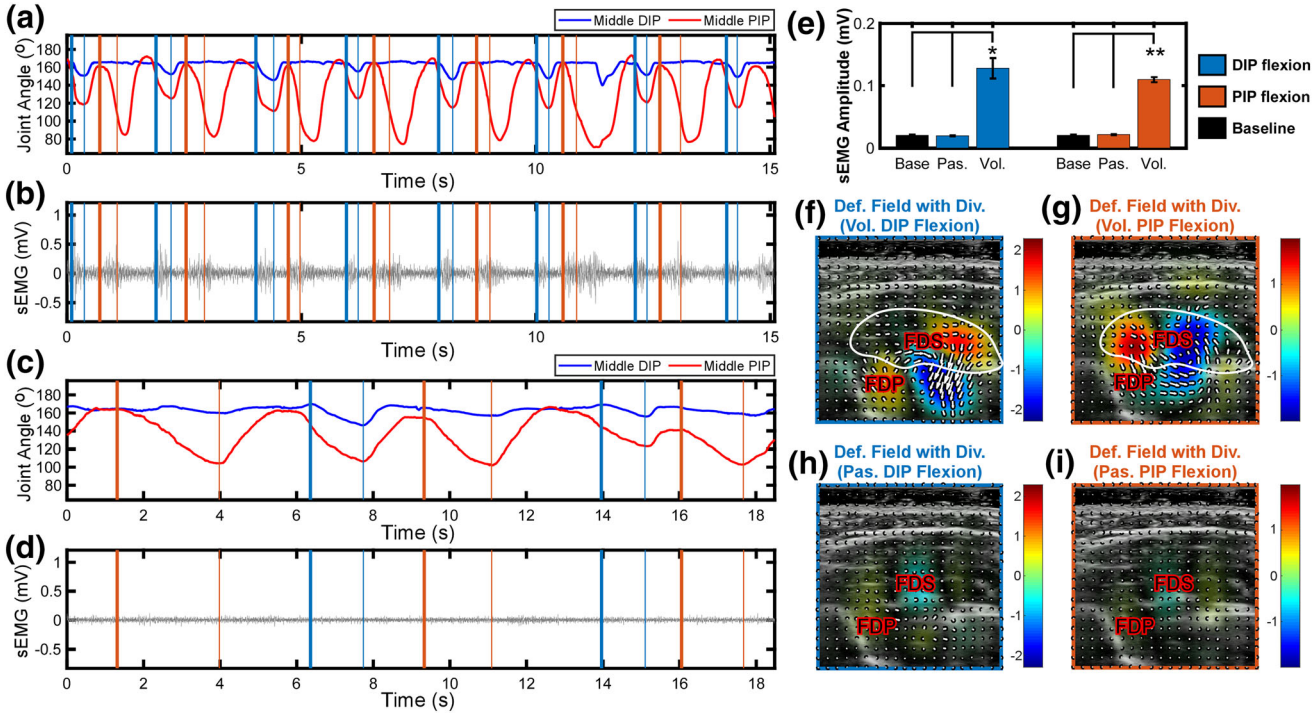

FIGURE 6. The joint kinematics (a) and sEMG signal (b) from the trial with voluntary PIP and DIP joint flexions alternately. The joint kinematics (c) and sEMG signal (d) from the trial with passive PIP and DIP joint flexions alternately. Orange thick and thin vertical lines represent the start and end of individual voluntary flexions of PIP joint, respectively, and blue thick and thin vertical lines represent the start and end of individual voluntary flexions of DIP joint, respectively (a, b, c, and d). The comparison of the sEMG amplitude (e). The ultrasound deformation field with the divergence from the voluntary DIP flexions (f) and PIP flexions (g). The ultrasound deformation field with the divergence from the passive DIP flexions (h) and PIP flexions (i). *$p < 0.01$, **$p < 0.0001$.

divergence of the deformation field to quantify the expansion or shrinkage of different areas to identify the activated muscles. The first experiment showed that our method can correctly identify the contracting muscles at both superficial and deep layers using concurrent intramuscular recordings. The second experiment demonstrated that our method is insensitive to passive muscle shortening.

Unlike the previous studies[3,10,11,20,29] in which longitudinal US images were used to estimate the muscle tissue movement along the fascicle direction, our algorithm utilized the transverse US images, which could detect the contracting regions of a group of muscles concurrently, by identifying the expanding or shrinking muscle regions. Compared with the longitudinal US images, the transverse US can capture the movements of different muscles simultaneously, which can be beneficial when multiple muscles need to be monitored concurrently, such as capturing different compartments of the extrinsic finger muscles during dexterous finger movements. Our method can also capture the activity of both deep and superficial muscles. For example, the sEMG recorded comparable activity level when FDP and FDS activated in an alternating manner. In contrast, the US images can individually capture the activity of these two muscles reliably (Figs. 5 and 6). The capacity to detect the muscle activity at different muscle depths also has potential clinical applications. Our method provides a potentially valuable tool to detect the contracting regions of different muscles concurrently, which can help to understand the mechanism of pathological conditions. For example, the altered coordination of the upper limb and hand post stroke[5,9] might result from the abnormal activation of multiple muscles. With further development, our method may serve as an assessment tool for clinicians to evaluate the function of muscles and the effect of treatments in individuals with neuromuscular disorders.

The results of the second experiment showed that the developed framework was insensitive to muscle passive shortening. First, since the joint motion speed was slow and no stretch reflex activity was elicited, the muscle deformation was small in the passive movement condition. In addition, the stepwise calculation of the deformation field could also average out inconsistent small movements of muscle tissues, resulting in a small muscle deformation field and therefore a small divergence value. In the current study, we only evaluated the finger muscles that have small sizes. As for the

muscles with large sizes such as the leg muscles, the muscle tissue displacements might be larger in the passive movement condition compared with the small finger muscles. Therefore, in future studies, we will also evaluate larger muscles to confirm that the developed method was not sensitive to passive shortening for muscles with different sizes.

In a previous study, the muscle activation level characterized by sEMG and muscle thickness measured using US was compared, and the results showed that the muscle thickness measured using US can be a reliable measurement of muscle activation level.[14] In the current study, we calculated the divergence of the deformation field to identify the contracting muscle regions. Since the divergence itself gives the quantity of the source of the deformation field, which should be related with the volume change of the muscle during contractions. The divergence has the potential to quantitatively characterize the muscle activation level. In further studies, the divergence of the muscle deformation field will be compared with the strength of the sEMG or iEMG signals at different contraction levels. In addition, the divergence of the muscle deformation field was not compared between the passive condition and the baseline condition when there were no joint flexions. Further development of our method can potentially provide a tool to visualize the muscle activation level on a US image in real-time.

In individuals with neuromuscular disorders, the muscle structure might be altered with decreased muscle cross-section, increased connective tissue or redistribution of collagen in the extracellular matrix. Since our method identifies the regions of contracting muscle by estimating the muscle tissue displacement, theoretically, the contracting muscles can still be identified as long as the muscle volume alters during contraction, resulting in muscle tissue displacement in the transverse plane. An earlier study showed that fascicle displacement was smaller in the affected muscles post-stroke during passive movement and voluntary movement.[18] In a previous study,[10] the abnormal muscle activation pattern with facioscapulohumeral muscular dystrophy was investigated by exploring the muscle tissue displacement along the longitudinal direction, which demonstrated the feasibility of tracking muscle tissue displacement with altered muscle structures. However, it still needs further verification on whether the estimation of the muscle tissue displacement in the transverse plane and the performance of the proposed method can be affected by the altered muscle structure. In addition, we will also investigate the ability of our method to reflect the abnormal muscle activation pattern by comparing with other measurements like electromyography in the future.

One limitation of the current study was that the developed framework was evaluated only in a limited number of subjects. As a preliminary study, the results showed that the developed method can automatically identify the contracting muscles in the transverse plane at different depths. The other limitation was that only finger muscles were captured. Compared with lower limb muscles, the finger muscles were significantly smaller. In our future studies, we plan to evaluate other muscles with different sizes in a larger subject sample to investigate the performance of the framework in a more extensive manner.

In conclusion, we developed a novel framework to detect the contracting muscles in the transverse US images. The algorithm includes mainly two steps. The first step estimates the muscle tissue movements in the transverse plane in a stepwise manner, resulting a deformation field. The second step calculates the divergence of the deformation field to identify expanding or shrinking regions that are typically resulted from the muscle contraction observed in the transverse plane. Two preliminary experiments were performed to evaluate the feasibility of the framework. The results showed that the developed framework can automatically detect the contracting muscles at different depths and could potentially complement other conventional methods in assessing the function of muscles such as EMG and kinetic measurements.

ELECTRONIC SUPPLEMENTARY MATERIAL

The online version of this article (https://doi.org/10.1007/s10439-020-02557-2) contains supplementary material, which is available to authorized users.

ACKNOWLEDGMENTS

This study was supported in part by the National Science Foundation (CBET-1847319).

CONFLICT OF INTEREST

The authors have no financial relationships that may cause a conflict of interest.

REFERENCES

[1]Akhlaghi, N., C. A. Baker, M. Lahlou, H. Zafar, K. G. Murthy, H. S. Rangwala, J. Kosecka, W. M. Joiner, J. J. Pancrazio, and S. Sikdar. Real-time classification of hand motions using ultrasound imaging of forearm muscles. *IEEE Trans. Biomed. Eng*. 63:1687–1698, 2015.

[2]Biały, M., W. Adamczyk, R. Gnat, and T. Stranc. Tissue deformation index as a reliable measure of lateral abdominal muscle activation on m-mode sonography. *J. Ultrasound Med.* 36:1461–1467, 2017.
[3]Bogaerts, S., C. D. B. Carvalho, L. Scheys, K. Desloovere, J. D'hooge, F. Maes, P. Suetens, and K. Peers. Evaluation of tissue displacement and regional strain in the achilles tendon using quantitative high-frequency ultrasound. *PLoS ONE* 12:e0181364, 2017.
[4]Bunce, S., A. Moore, and A. Hough. M-mode ultrasound: a reliable measure of transversus abdominis thickness? *Clin. Biomech.* 17:315–317, 2002.
[5]Carpinella, I., J. Jonsdottir, and M. Ferrarin. Multi-finger coordination in healthy subjects and stroke patients: a mathematical modelling approach. *J. Neuroeng. Rehabil.* 8:19, 2011.
[6]Castellini, C., G. Passig, and E. Zarka. Using ultrasound images of the forearm to predict finger positions. *IEEE Trans. Neural Syst. Rehab. Eng.* 20:788–797, 2012.
[7]Chen, X., Y.-P. Zheng, J.-Y. Guo, Z. Zhu, S.-C. Chan, and Z. Zhang. Sonomyographic responses during voluntary isometric ramp contraction of the human rectus femoris muscle. *Eur. J. Appl. Physiol.* 112:2603–2614, 2012.
[8]Chleboun, G. S., A. R. France, M. T. Crill, H. K. Braddock, and J. N. Howell. In vivo measurement of fascicle length and pennation angle of the human biceps femoris muscle. *Cells Tissues Organs* 169:401–409, 2001.
[9]Debaere, F., D. Van Assche, C. Kiekens, S. Verschueren, and S. Swinnen. Coordination of upper and lower limb segments: deficits on the ipsilesional side after unilateral stroke. *Exp. Brain Res.* 141:519–529, 2001.
[10]Gijsbertse, K., R. Goselink, S. Lassche, M. Nillesen, A. Sprengers, N. Verdonschot, N. van Alfen, and C. De Korte. Ultrasound imaging of muscle contraction of the tibialis anterior in patients with facioscapulohumeral dystrophy. *Ultrasound Med. Biol.* 43:2537–2545, 2017.
[11]Gooch, C. L., T. J. Doherty, K. M. Chan, M. B. Bromberg, R. A. Lewis, D. W. Stashuk, M. J. Berger, M. T. Andary, and J. R. Daube. Motor unit number estimation: a technology and literature review. *Muscle Nerve* 50:884–893, 2014.
[12]Guo, J.-Y., Y.-P. Zheng, H.-B. Xie, and X. Chen. Continuous monitoring of electromyography (emg), mechanomyography (mmg), sonomyography (smg) and torque output during ramp and step isometric contractions. *Med. Eng. Phys.* 32:1032–1042, 2010.
[13]Kamavuako, E. N., D. Farina, K. Yoshida, and W. Jensen. Estimation of grasping force from features of intramuscular emg signals with mirrored bilateral training. *Ann. Biomed. Eng.* 40:648–656, 2012.
[14]Kim, C.-Y., J.-D. Choi, S.-Y. Kim, D.-W. Oh, J.-K. Kim, and J.-W. Park. Comparison between muscle activation measured by electromyography and muscle thickness measured using ultrasonography for effective muscle assessment. *J. Electromyogr. Kinesiol.* 24:614–620, 2014.
[15]Mademli, L., and A. Arampatzis. Behaviour of the human gastrocnemius muscle architecture during submaximal isometric fatigue. *Eur. J. Appl. Physiol.* 94:611–617, 2005.
[16]McMeeken, J., I. Beith, D. Newham, P. Milligan, and D. Critchley. The relationship between emg and change in thickness of transversus abdominis. *Clin. Biomech.* 19:337–342, 2004.
[17]Mogk, J. P., and P. J. Keir. Crosstalk in surface electromyography of the proximal forearm during gripping tasks. *J. Electromyogr. Kinesiol.* 13:63–71, 2003.
[18]Nelson, C. M., W. M. Murray, and J. P. A. Dewald. Motor impairment-related alterations in biceps and triceps brachii fascicle lengths in chronic hemiparetic stroke. *Neurorehabil. Neural Repair* 32:799–809, 2018.
[19]Perry, J., C. S. Easterday, and D. J. Antonelli. Surface versus intramuscular electrodes for electromyography of superficial and deep muscles. *Phys. Ther.* 61:7–15, 1981.
[20]Revell, J., M. Mirmehdi, and D. McNally. Musculoskeletal motion flow fields using hierarchical variable-sized block matching in ultrasonographic video sequences. *J. Biomech.* 37:511–522, 2004.
[21]Shi, J., J.-Y. Guo, S.-X. Hu, and Y.-P. Zheng. Recognition of finger flexion motion from ultrasound image: a feasibility study. *Ultrasound Med. Biol.* 38:1695–1704, 2012.
[22]Shin, H., Y. Zheng, and X. Hu. Variation of finger activation patterns post-stroke through non-invasive nerve stimulation. *Front. Neurol.* 9:1101, 2018.
[23]Simon, N. G. Dynamic muscle ultrasound-another extension of the clinical examination. *Clinical neurophysiology: official journal of the International Federation of Clinical Neurophysiology* 126:1466, 2015.
[24]Simon, N. G., Y.-I. Noto, and C. M. Zaidman. Skeletal muscle imaging in neuromuscular disease. *J. Clin. Neurosci.* 33:1–10, 2016.
[25]Smith, L. H., T. A. Kuiken, and L. J. Hargrove. Real-time simultaneous and proportional myoelectric control using intramuscular emg. *J. Neural Eng.* 11:066013, 2014.
[26]Solomonow, M., R. Baratta, M. Bernardi, B. Zhou, Y. Lu, M. Zhu, and S. Acierno. Surface and wire emg crosstalk in neighbouring muscles. *J. Electromyogr. Kinesiol.* 4:131–142, 1994.
[27]Stokes, I. A., S. M. Henry, and R. M. Single. Surface emg electrodes do not accurately record from lumbar multifidus muscles. *Clin. Biomech.* 18:9–13, 2003.
[28]Thirion, J.-P. Image matching as a diffusion process: an analogy with maxwell's demons. *Med. Image Anal.* 2:243–260, 1998.
[29]van der Werff, R., S. O'Leary, G. Jull, M. Peolsson, J. Trygg, and A. Peolsson. A speckle tracking application of ultrasound to evaluate activity of multilayered cervical muscles. *J. Rehabil. Med.* 46:662–667, 2014.
[30]Vercauteren, T., X. Pennec, A. Perchant, and N. Ayache. Diffeomorphic demons: efficient non-parametric image registration. *Neuroimage* 45:S61–S72, 2009.
[31]Zheng, Y., and X. Hu. Reduced muscle fatigue using kilohertz-frequency subthreshold stimulation of the proximal nerve. *J. Neural Eng.* 15:066010, 2018.
[32]Zheng, Y., and X. Hu. Elicited finger and wrist extension through transcutaneous radial nerve stimulation. *IEEE Trans. Neural Syst. Rehab. Eng.* 27:1875–1882, 2019.